Available online at www.sciencedirect.com
ScienceDirect
Polymer 47 (2006) 8123–8136
polymer
www.elsevier.com/locate/polymer

Properties and morphology of nanocomposites based on styrenic polymers. Part I: Styrene-acrylonitrile copolymers

H.A. Stretz [a,*], D.R. Paul [b]

[a] Department of Chemical Engineering, Tennessee Technological University, Cookeville, TN 38505, USA
[b] Department of Chemical Engineering and Texas Materials Institute, University of Texas at Austin, Austin, TX 78712, USA

Received 19 August 2006; received in revised form 21 September 2006; accepted 24 September 2006
Available online 18 October 2006

Abstract

For polymer/organoclay nanocomposites formed by melt processing, interactions between the polymer, montmorillonite surface, and surfactant determine any thermodynamic driving force for dispersion of the clay in the polymer. Interactions between poly(styrene-*co*-acrylonitrile) (SAN) and a single organoclay were probed by varying the SAN copolymer composition. Sample preparation was accomplished by melt processing on a microcompounder followed by injection molding. The level of mechanical reinforcement was observed to increase with acrylonitrile content. Digital analyses of TEM photomicrographs of core samples suggest an optimum in the aspect ratio of the particles at ~38 wt% acrylonitrile; montmorillonite particles are much longer and thicker for the PS-based composites indicting poor exfoliation compared to the SAN-based composites. The melt viscosity of the SAN copolymers used in this work increased with AN content; experiments showed that varying melt viscosity independent of AN content can account for some improvement in reinforcement.

Keywords: SAN; Montmorillonite; Nanocomposite

1. Introduction

For polymer nanocomposites formed from montmorillonite-based organoclays (MMT) made by melt processing, the interaction between the polymer and the organoclay is an important factor that affects how well the clay particles are dispersed. In a previous paper, we examined the relationship between organoclay surfactant structure and clay particle morphology in styrene-acrylonitrile copolymer (SAN)/MMT composites prepared in a twin-screw extruder [1]. Another way to affect the polymer–organoclay interaction is to vary the structure of the polymer itself in a systematic manner. By adjusting the acrylonitrile (AN) composition in an SAN copolymer, the number of polar groups available for polymer–surfactant and polymer–silicate surface interactions can be varied. In this work, SAN copolymers that contained 0–58% by weight of AN were used to form melt-blended nanocomposites in order to probe a wide range of interactions.

Descriptions of nanocomposite morphology and dispersion have traditionally relied on the complementary techniques of wide angle X-ray scattering (WAXS) and transmission electron microscopy (TEM). A shift in the WAXS d_{001}-spacing (defined as $\Delta d_{001} = d_{001,\text{composite}} - d_{001,\text{organoclay}}$) has usually been interpreted in terms of polymer intercalation into the organoclay galleries, and the absence of an X-ray peak has frequently been misinterpreted to mean a high state of exfoliation [2], although other morphological states may also lead to similar X-ray signals. TEM analysis yields very direct information about particle morphology but reflects only a localized scale. Use of digital analysis and random sampling from a range of locations enhances the value of the TEM information [3].

Mechanical properties such as tensile modulus can be a good indicator of particle dispersion in addition to being an important measure of performance. Increasing dispersion results in an increased average aspect ratio for montmorillonite particles and greater potential to reinforce. The effect of particle

* Corresponding author. Tel.: +1 931 372 3495; fax: +1 931 372 6352.
E-mail address: hstretz@tntech.edu (H.A. Stretz).

0032-3861/$ - see front matter © 2006 Elsevier Ltd. All rights reserved.
doi:10.1016/j.polymer.2006.09.049

dispersion on composite modulus has been shown to agree relatively well with predictions by traditional composite models such as those by Halpin–Tsai and Mori–Tanaka for well-dispersed systems, *e.g.*, nylon 6/MMT [4,5]. However, reinforcement data are known to be affected by the modulus of the matrix component, and these composite models, as recently discussed [6,7], provide a useful basis to account for such effects. In the current study the matrix moduli of the various composites change, and we therefore consider the matrix modulus effect and potential for reinforcement in a given matrix.

Another factor of the SAN copolymers available for this study is that the melt viscosity of the polymer matrix increases as their AN content increases. Fornes et al. showed that melt viscosity of the matrix affects the extent of exfoliation for melt-processed nylon 6 nanocomposites [8], presumably because of the shear stresses exerted on the particle during mixing. The effect of shear stress on dispersion must, therefore, be explored in order to separate its contribution from that of the potential attractions between the polar acrylonitrile and the organoclay.

The scope of this paper is to examine the effect of AN content of SAN copolymers on the morphology and properties of nanocomposites formed from a single organoclay, montmorillonite modified with trimethyl octadecyl ammonium surfactant. This organoclay modifier was chosen to build upon previous results, in which SAN containing 25 wt% acrylonitrile was extrusion-mixed with a variety of organoclays [1] and the trimethyl octadecyl ammonium-based organoclay produced a high composite reinforcement effect in these studies. All materials were melt-mixed using a twin-screw microcompounder and analyzed using TEM/digital image analysis, WAXS, and tensile modulus. The importance of the melt viscosity on exfoliation during mixing is also discussed.

2. Previous work on styrenic nanocomposites

The two extremes of acrylonitrile composition in SAN copolymers are polyacrylonitrile (PAN) and polystyrene (PS). PAN composites with montmorillonite require in situ polymerization, such as in reports by Chung and Choi [9] and Choi et al. [10], since PAN is not thermally stable enough to melt process. Efforts to form PS/MMT nanocomposites have been extensively described in the literature; generally melt-processed versions seem to lead to less exfoliation than those formed by well-designed in situ polymerization processes with surfactants for the organoclay that can serve as initiators for the polymerization [11–13]. Morgan et al. have reported that improved dispersion is achieved with dilution of the polymer in a solvent aided by sonication [14]. Studies of nanocomposites formed in melt processes seem to suggest slightly better dispersion the lower the PS molecular weight [15,16], and the lower the molecular weight of the clay surfactant [17,18]. Robello et al. [19] used star-shaped polystyrene as the matrix and the TEM images show reasonable dispersion after heating in the melt state for 24 h.

In general, several authors have investigated the effect of styrenic copolymer structure on composites with MMT, as we previously reviewed [1]. Morgan et al. [20], Ko [21], and Goettler and Nagaraj [22] have discussed the effect of AN content on SAN nanocomposites, and WAXS and flexural modulus information reported by these authors suggest that exfoliation may increase with AN content.

3. Experimental

3.1. Materials

The SAN copolymers used are described in Table 1. The montmorillonite organoclay was supplied by Southern Clay Products. The native, negatively charged montmorillonite clay platelets, typically with counterbalancing sodium ions, have a cation exchange capacity (CEC) of about 92 mequiv/100 g. The organoclay was formed by ion-exchange with a trimethyl octadecyl ammonium surfactant by the supplier at 95 mequiv/100 g. Thus, organic ammonium ions have been exchanged for the sodium cations of the organoclay approximately in a stoichiometric ratio. The mass loss on ignition, 30%, is representative of the amount of organic surfactant contained by the organoclay; this experimentally determined value also includes a small contribution from the rearrangement of the silicate structure when exposed to very high temperatures [23].

Table 1
Description of matrix materials

Material	Supplier	Trade name	M_w (g/mol)	% AN	T_g (°C)	Plateau force on microcompounder screws[a] (N)	Young's modulus (GPa)	Density (g/cm^3)
PS	Dow Chemical	Styron 678 CW		0		689	2.92	1.04
PS	Dow Chemical	Styron 685 D	300,000	0	102	998	3.13	1.04
SAN-2	Asahi	Experimental	204,000	2	108	956	3.03	1.04[b]
SAN-13.5	Asahi	Experimental	149,000			1133	3.17	1.06[b]
SAN-25	Dow Chemical	Tyril 100	152,000	25	107	1465	3.24	1.07
SAN-27 M80	Bayer			27		1819	3.33	1.08[b]
SAN-31	Dow Chemical	Tyril 125	98,000	31		1580	3.27	1.08[b]
SAN-38	Monsanto	Experimental		38		2079	3.47	1.09[b]
SAN-58	Monsanto	Experimental		58	116	2604	3.73	1.12

[a] Values measured at 220 °C, 100 rpm and 1.5 mm gap after 10 min.
[b] Values are estimates from a linear fit of density data for copolymers of varying AN content.

3.2. Methods

All materials were dried overnight under vacuum at 80 °C prior to use. Powdered polymer and powdered organoclay were weighed and hand-mixed to form a homogenous masterbatch and 3.2 g portions of this masterbatch were then fed into a microcompounder (manufactured by DSM, 5 cm^3 batch capacity, with intermeshing co-rotating twin screws tapering in diameter from 1 cm to 0.43 cm along their length of 10.75 cm). This type of microcompounder was necessary for this study because of the limited availability of some of the SAN copolymers.

Polymer and organoclay were then melt blended for 10 min. The mixing was done primarily at 100 rpm and a barrel temperature of 220 °C at a 1.5 mm gap between the extrusion chamber and rest stop. In some cases, the screw speed was varied up to 380 rpm, and the data are labeled accordingly. The turnover rate for SAN-25 in the microcompounder under these conditions has been estimated as four times per minute. The axial force developed by the screws as they rotate was recorded during the mixing process as a function of time, and values reported are averages of the last three readings, 30 s apart, at 8–10 min residence time, when the force had reached a plateau. The force readout on this instrument is used as a measure of the mixture melt viscosity, as opposed to the standard torque sensor commonly found on larger-scale batch compounders.

After the 10 min residence time, material was melt pumped into a heated transfer device, at 225 °C, and then injection molded using a bench top pneumatic ram injection molder at an injection pressure of 60 psi. Time to fill the mold varied from 0.25 s for the PS/MMT composites to 0.84 s for the SAN-58/MMT composites. The mold possessed a film-type gate and was heated to 80 °C. Parts were cooled for 5 min prior to opening the mold. The molded part was rectangular, measuring 0.155 × 0.4 × 3.1 cm, with dimensions very similar to an Izod bar (ASTM D638) but half the normal length.

Tensile modulus was measured on an Instron model 1137 at a crosshead rate of 0.51 cm/min using an extensometer having a 2.54 cm gage length. Because the specimens were rectangular and not dog bone-shaped, strength values could not be determined; and specimens were not allowed to proceed to failure during the test. Modulus was measured five times for each specimen, with no single test exceeding 1% strain. No evidence of hysteresis was observed and modulus values on a single specimen were repeatable within a maximum of 2% standard deviation. Three specimens per sample were tested, with standard deviations for modulus at a maximum of 5% of the mean.

The aluminosilicate percentages (%MMT) were determined from the ash content of dry microcompounder extrudate that was heated at 900 °C for over 45 min. The weight percent of aluminosilicate content in each sample (%MMT) was calculated from the ash concentration ($\%MMT_{ash}$) by the following equation,

$$\%MMT = \frac{\%MMT_{ash}}{0.935} \quad (1)$$

where the "0.935" factor corrects for structural rearrangements of the pristine montmorillonite at such temperatures.

WAXS scans were obtained using a Scintag XDS 2000 diffractometer. Injection-molded samples were scanned such that the beam probed the skin of the tensile bar perpendicular to the direction of flow. For certain samples, identified as such in the text, the skin of the bar was removed by an automated milling machine prior to the WAXS scan in order to obtain information about the morphology in the core of the bar.

Thin sections for microscopy were prepared using a Reichert–Jung Ultracut E cryogenic ultramicrotome at a nominal thickness of 50 nm with the knife at room temperature. Knife speeds were 0.3–0.5 mm/s. The sections were imaged using a JEOL 2010 F electron microscope operating at 120 kV.

The convention used for describing directions of TEM image planes and orientations of particles follow from a frame of reference set by the direction of material flow during molding, as shown in Fig. 1. The convention for identifying a plane is to specify its normal vector, *i.e.*, the direction along which the image is viewed describes the plane of the image. Specimens were prepared for this study such that images could be viewed both along the flow direction (FD) and along the transverse direction (TD). It is important to note the orientation of the particles in the plane of an image, *i.e.*, for images viewed along the transverse direction, the organoclay particles tend to be oriented along the flow direction axis.

Image analysis was performed on digitally captured images, using 350–400 particles from 8 to 30 photomicrographs. Gatan DigitalMicrograph analysis software was employed to measure the length, thickness, and angle of orientation for each particle.

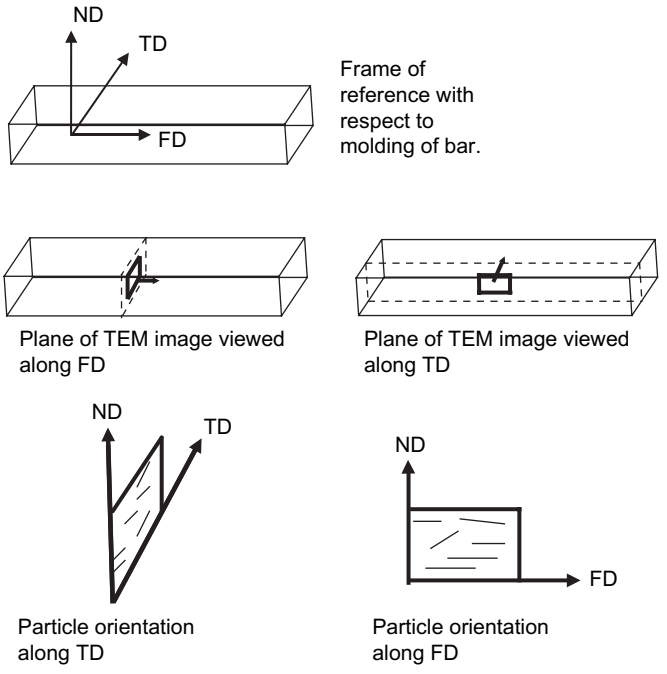

Fig. 1. Conventions for description of TEM photomicrograph image plane and description of orientation of particles observed in those images. The direction of flow during injection molding is used as a frame of reference. FD = flow direction, TD = transverse direction, and ND = normal direction.

4. Effect of copolymer composition on particle morphology

4.1. Transmission electron microscopy

Representative TEM photomicrographs showing the morphology of some of the copolymer nanocomposites containing 3.2% MMT are compared qualitatively in this section. Fig. 2 shows a series of low magnification TEM images where AN content of the copolymer matrix is varied. This overview demonstrates that the PS and SAN-2-based nanocomposites contain very large tactoids, but the particle size decreases and particle density increases for materials with higher AN content. TEM images at higher magnifications are presented next. Those viewed along the transverse direction in this series are shown initially (part a and b in Figs. 3–8) because the particles in these images are oriented along the axis of the applied testing load, and the particle dimensions along this axis are important when predicting the composite modulus; see Fig. 1 for comparison of view direction and particle direction.

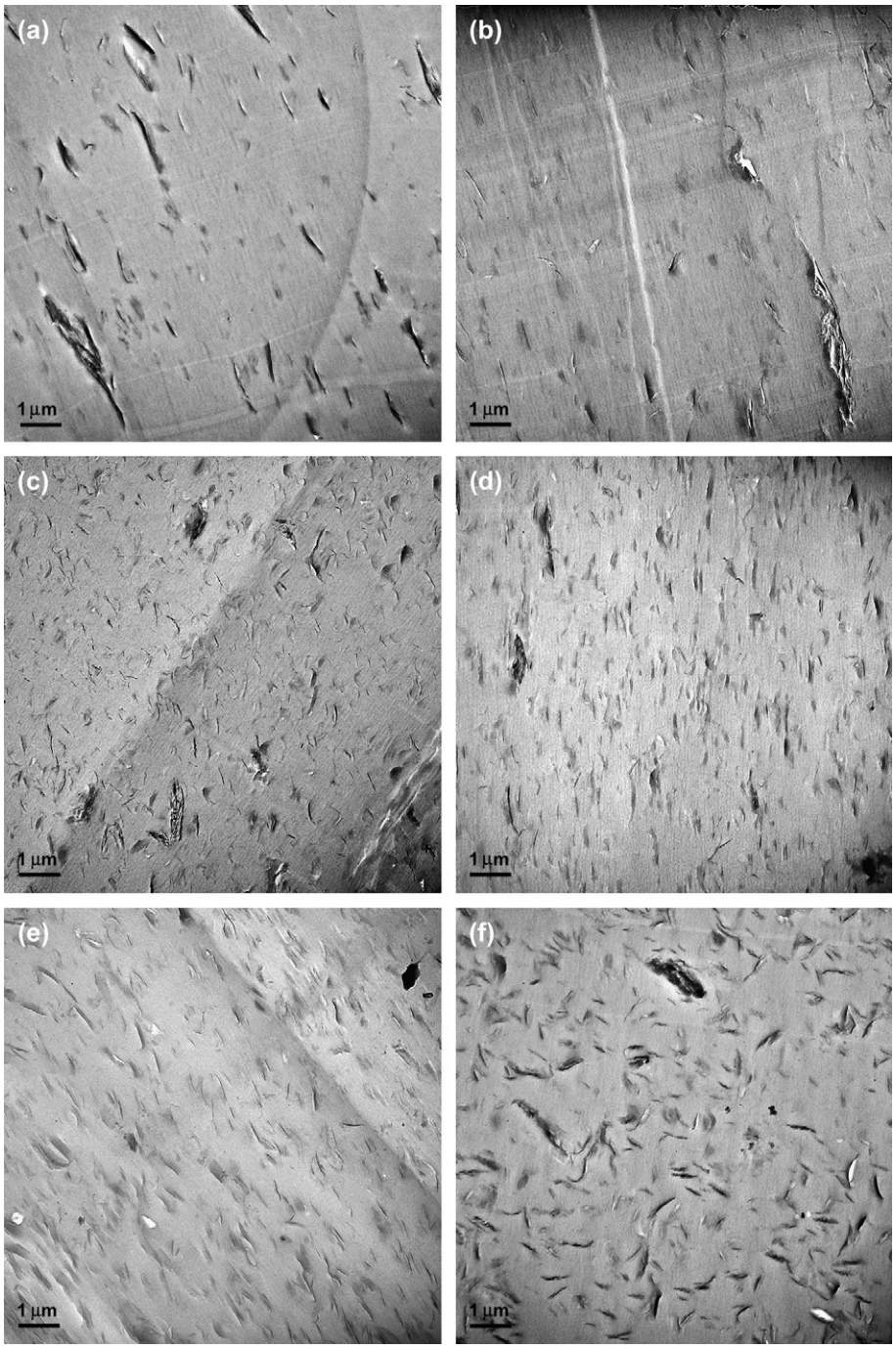

Fig. 2. TEM photomicrographs viewed along the transverse direction (TD) at low magnification, 3000×, for the nanocomposites based on (a) PS, (b) SAN-2, (c) SAN-13.5, (d) SAN-25, (e) SAN-38, and (f) SAN-58.

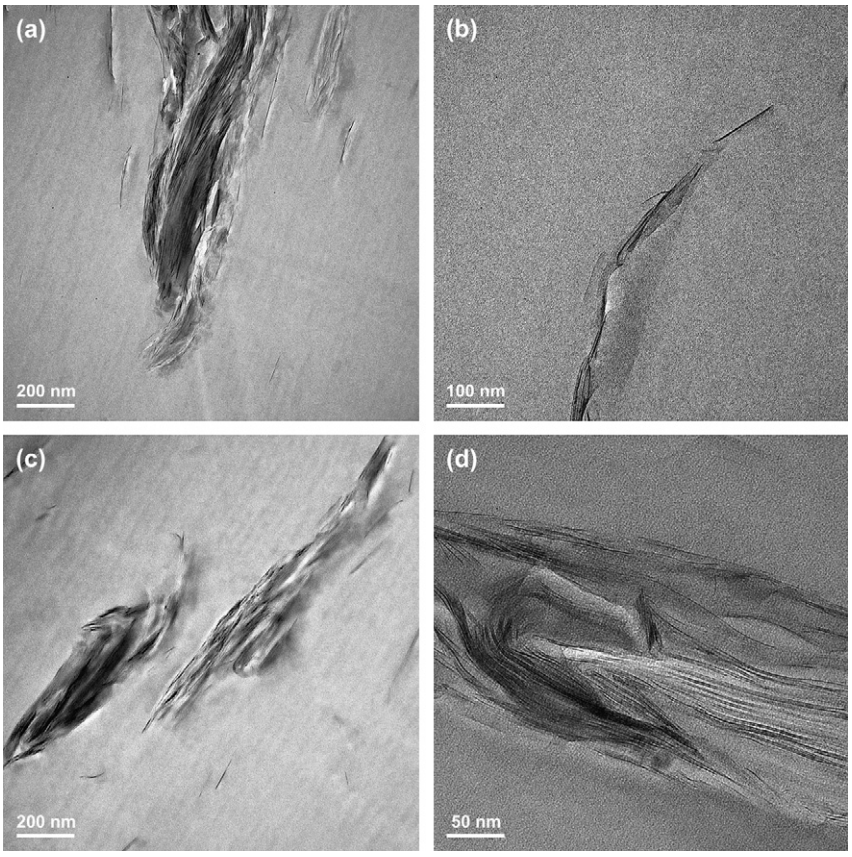

Fig. 3. TEM photomicrographs of the PS/$M_3(C_{18})_1$ composite, 3.2% MMT, viewed along (a, b) the transverse direction (TD) and (c, d) the flow direction (FD).

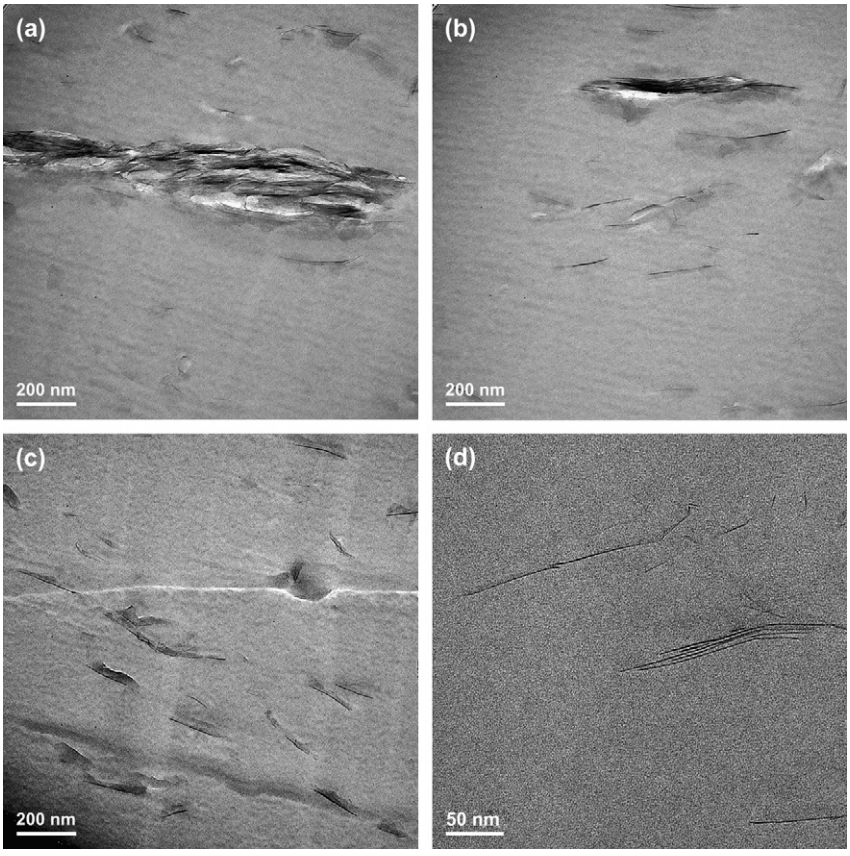

Fig. 4. TEM photomicrographs of the SAN-2/$M_3(C_{18})_1$ composite, 3.2% MMT, viewed along the transverse direction (TD).

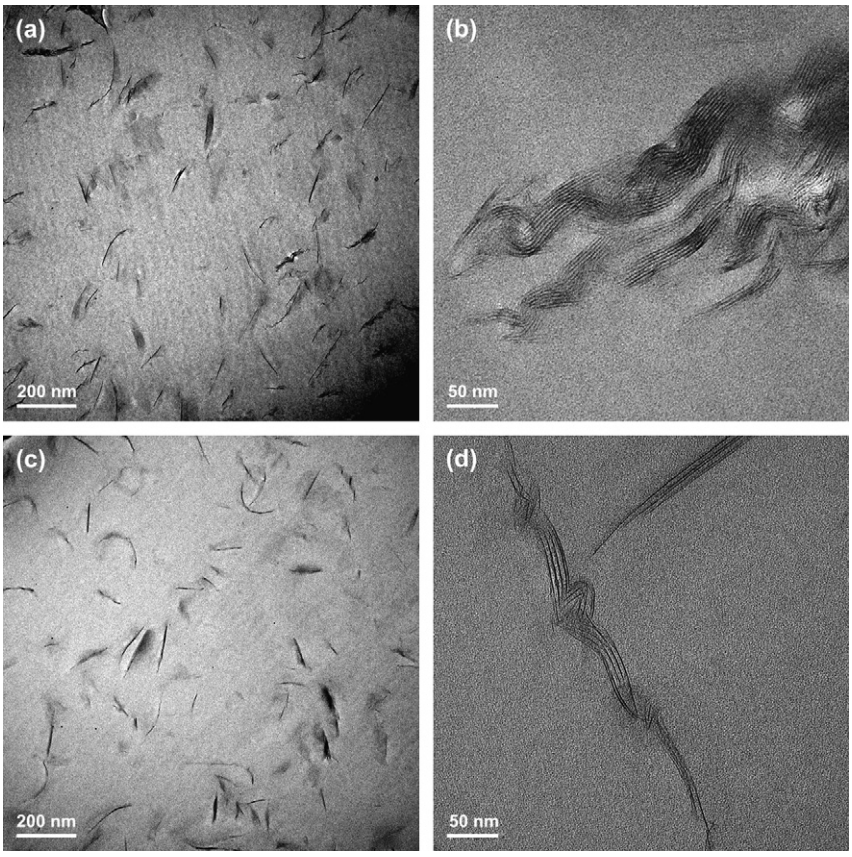

Fig. 5. TEM photomicrographs of the SAN-13.5/$M_3(C_{18})_1$ composite, 3.2% MMT, viewed along (a, b) the transverse direction (TD) and (c, d) the flow direction (FD).

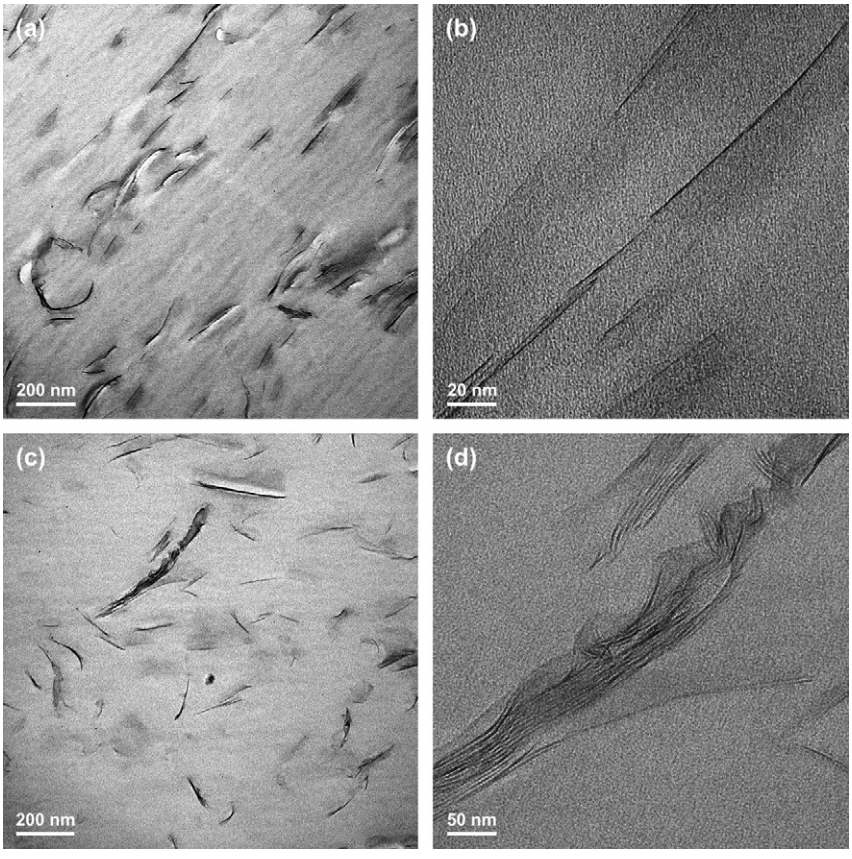

Fig. 6. TEM photomicrographs of the SAN-25/$M_3(C_{18})_1$ composite, 3.2% MMT, viewed along (a, b) the transverse direction (TD), and (c, d) the flow direction (FD).

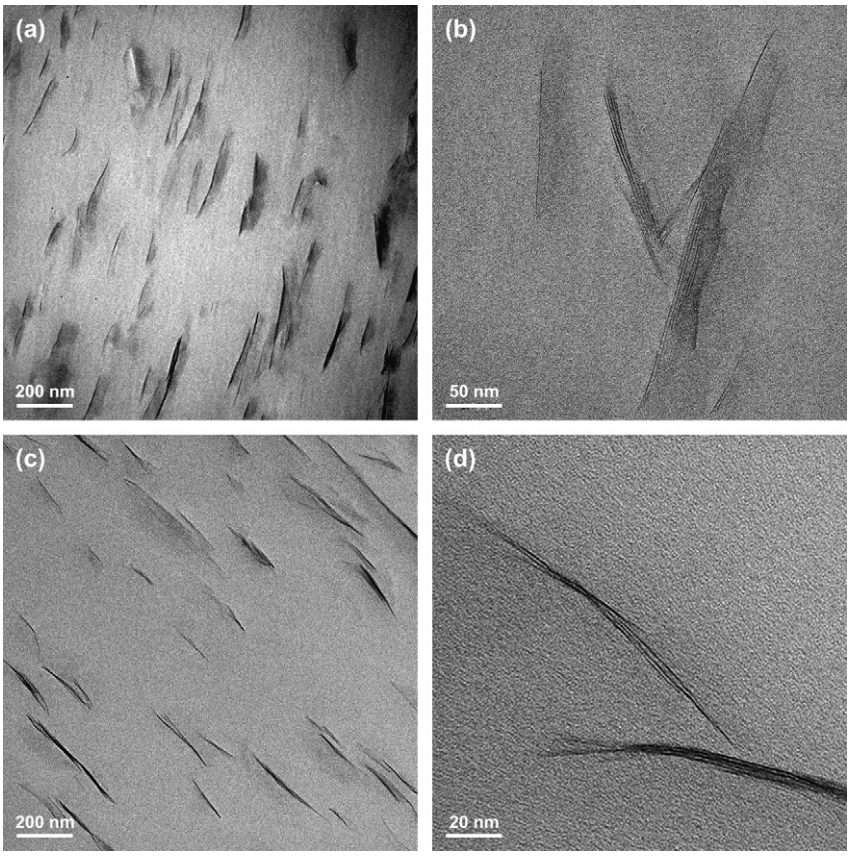

Fig. 7. TEM photomicrographs of the SAN-38/$M_3(C_{18})_1$ composite, 3.2% MMT, viewed along (a, b) the transverse direction (TD) and (c, d) the flow direction (FD).

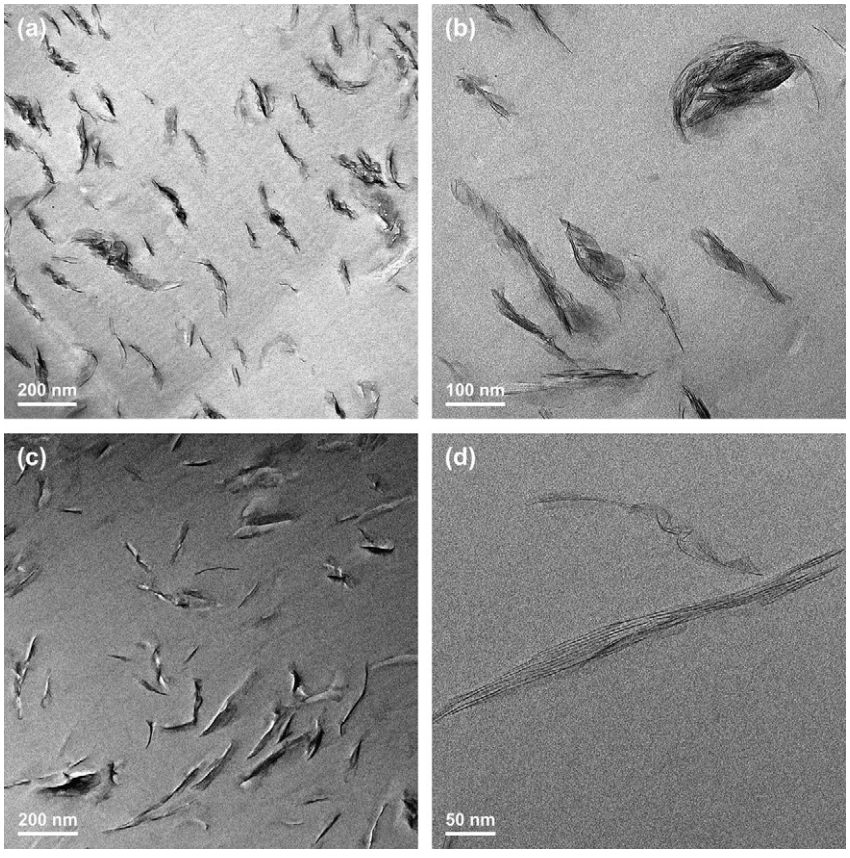

Fig. 8. TEM photomicrographs of the SAN-58/$M_3(C_{18})_1$ composite, 3.2% MMT, viewed along (a, b) the transverse direction (TD) and (c, d) the flow direction (FD).

TEM photomicrographs viewed along the flow direction are also presented for comparison (part c and d in Figs. 3–8). The results of digital image analysis applied to multiple images at 10 K magnification are presented in Section 4.1.1.

TEM images for the PS-based and SAN-2-based composites are shown in Figs. 3 and 4, respectively. The large MMT particles shown for both materials are comprised of hundreds of platelets. While Fig. 3c and d are flow direction views for the PS-based material, all four images in Fig. 4 for the SAN-2 based material are transverse views in an attempt to represent the heterogeneity of dispersion exhibited by both PS and SAN-2 composites. Distances between the larger particles in both cases are in the order of microns. The internal morphology of these large particles is complex, consisting of agglomerates of tactoids exhibiting significant disorder. A limited number of smaller particles (~3–6 platelets) are present in the matrix along with the larger particles, and there appear to be slightly more of these smaller particles in the SAN-2-based material.

TEM photomicrographs for the SAN-13.5, SAN-25 and SAN-38 nanocomposites are presented in Figs. 5–7, respectively. The particle density is significantly higher in these materials than for the PS-based or SAN-2-based composites. The orientation of the particles appears to improve as AN content increases.

The SAN-58 material, as seen in Fig. 8, exhibits more random particle orientations than the other SAN-based composites. The shapes of these particles are more irregular compared to the other SAN-based nanocomposites, as well as more irregular when viewed along the transverse direction.

Overall, the most significant difference noted in this series of images is that materials with AN contents of 13.5 wt% or greater show improved exfoliation, marked by smaller particle thicknesses and greater particle densities compared to the PS-based or SAN-2-based composites. The SAN-58-based nanocomposite exhibits irregular particle shapes compared to the other SAN-based nanocomposites. Also note that the ends of the particles in all composites are generally tapered compared to the particle's middle, *i.e.*, there are few particles which are splayed at the ends.

4.1.1. Digital image analysis

Table 2 gives the results of digital image analysis. Averages for particle length, thickness, aspect ratio, orientation and particle density are reported using images viewed along both the transverse and flow directions.

Number average particle lengths and thicknesses for these materials are presented as a function of copolymer composition in Fig. 9. Here, particle thickness appears to be approximately constant for all of the SAN-based composites and particle length appears to increase slightly when viewed along the flow direction for AN content between 13 and 38%. The distribution for the PS-based composite contains particles that are much thicker than observed for the other materials. These particles are also much longer than seen for the copolymers containing acrylonitrile.

The values reported for average aspect ratio in Table 2 are computed from the image analysis files in two different ways. In previous publications, data files for particle length and particle thickness were collected separately, a method which is more suitable for well-exfoliated materials. In these cases the aspect ratio was calculated as a ratio of two averages, *i.e.*,

$$\mathrm{AR} = \frac{(\bar{l})_n}{(\bar{t})_n} \tag{2}$$

Table 2
Image analysis of TEM photomicrographs

Copolymer	Number average length (nm, $\bar{l}_n$)	Number average thickness (nm, $\bar{t}_n$)	Estimated number of platelets per stack	Aspect Ratio, $\bar{l}_n/\bar{t}_n$	Number averge aspect ratio, $\langle l/t\rangle_n$	TEM particle density[a] (μm^{-2})	Specific particle density[b] (particles/μm^2)	Average particle deviation from mean angle of orientation (degrees, $\langle\Delta\alpha\rangle = \langle|\bar{\alpha} - \alpha|\rangle$)
Images viewed along transverse direction[d]								
PS	205	10.8	4.1	19.0	40.6	6.4	2.0	17.8
SAN-2	150	6.2	2.7	24.3	38.3	8.7	2.7	45.3
SAN-13.5	123	5.0	2.3	24.5	32.1	19.3	6.0	27.5
SAN-25	171	6.1	2.7	28.0	35.7	16.1	5.0	12.9
SAN-38	151	5.4	2.4	27.9	37.1	21.2	6.7	15.6
SAN-58[c]	149	10.7	4.1	14.0	23.0	25.9	8.1	23.5
Images viewed along flow direction[d]								
PS	276	14.9	5.5	18.5	41.3	3.88	1.2	26.2
SAN-13.5	126	6.1	2.7	20.6	27.1	20.0	6.3	46.7
SAN-25	148	5.6	2.5	26.5	38.3	16.5	5.2	56.9
SAN-27	118	4.7	2.2	25.4	35.6	27.1	8.5	50.9
SAN-38	182	5.3	2.4	34.1	46.4	26.5	8.3	10.1
SAN-58[c]	168	6.5	2.8	25.9	39.1	16.7	5.2	32.6

[a] The TEM particle density is the average number of montmorillonite particles per μm^2.
[b] The specific particle density is the (TEM particle density)/(MMT concentration), where MMT = 3.2 wt%.
[c] SAN-58 TD photomicrographs showed predominately twisted, perturbed particles.
[d] Particles oriented along the flow direction were taken from images viewed along the transverse direction and *vice versa*.

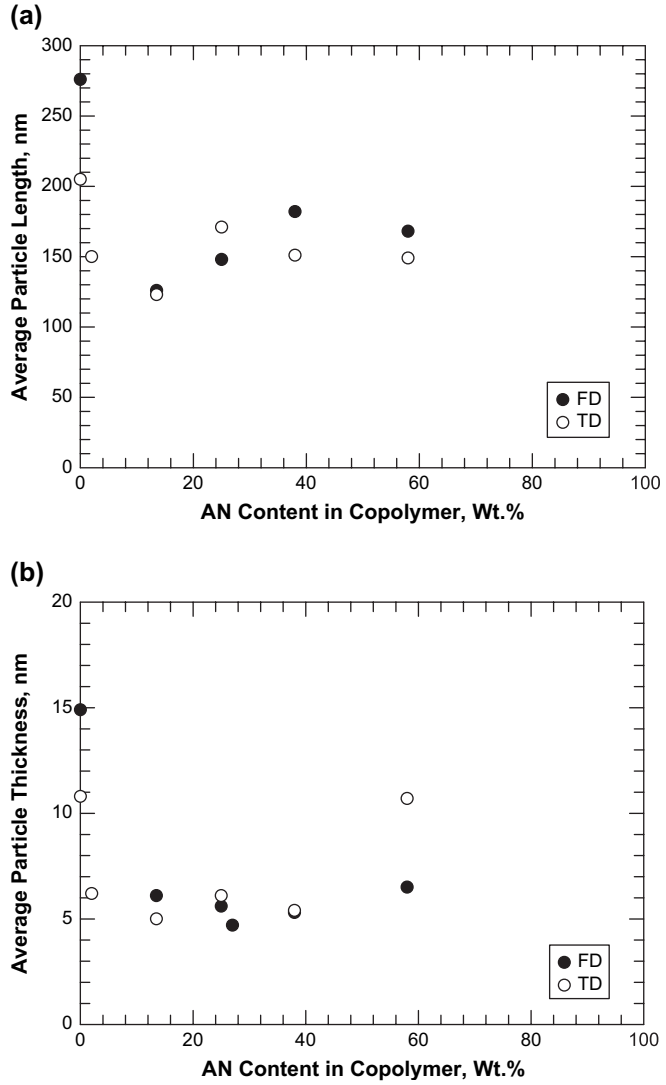

Fig. 9. TEM-based number average values *versus* acrylonitrile content in the copolymer for (a) particle length and (b) particle thickness.

Another method that is easily used for not so well-exfoliated systems is to collect a file of the individual particle aspect ratios and then compute an average as follows.

$$\mathrm{AR} = \left\langle \frac{l}{t} \right\rangle_n = \frac{\sum n_i \left(\frac{l}{t}\right)_i}{n} \tag{3}$$

Both types of calculations are presented in order to provide a basis for comparison of particle morphologies with information published previously, specifically for comparison to nylon 6 nanocomposites [4].

The results in Table 2 show that $\langle l/t \rangle_n$ values are significantly higher than $(\bar{l})_n/(\bar{t})_n$ in all cases. The $\langle l/t \rangle_n$ values are plotted in Fig. 10, and there appears to be a slight maximum for an acrylonitrile content of around 38 wt%. Aspect ratios for the SAN-38 and SAN-58 nanocomposites are greater when viewed in the flow direction.

While particle aspect ratios viewed along the transverse direction are relevant to predict tensile modulus of the composite, various important properties such as the coefficient

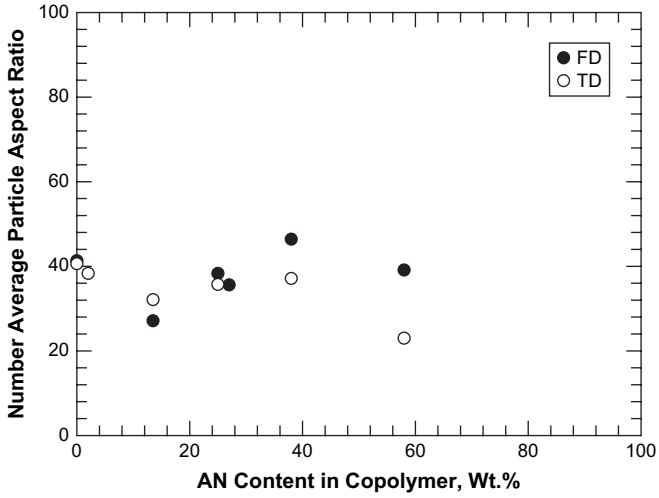

Fig. 10. TEM-based number average particle aspect ratio *versus* acrylonitrile content in the copolymer. FD = TEM image viewed along the flow direction, TD = TEM image viewed along the transverse direction.

of thermal expansion require information about aspect ratios viewed along the flow direction as well. Fig. 11 shows histograms of the individual particle aspect ratios for the SAN-25/MMT composite as viewed along the flow direction and transverse direction, and these distributions are substantially the same. This agreement between aspect ratio distributions was true for the PS and SAN-13.5-based nanocomposites as well. The SAN-58-based nanocomposite particles, however, appeared to have higher aspect ratios when viewed in the flow direction, as shown in Fig. 12 (Although not depicted in Fig. 12, the SAN-38-based nanocomposite particles also showed this trend.). This discrepancy for the SAN-58 materials may be an artifact of the difficulty in measuring the thickness of an irregularly-shaped particle, the predominant type of particle morphology for this nanocomposite. For the SAN-38 materials, however, the aspect ratio difference in the two

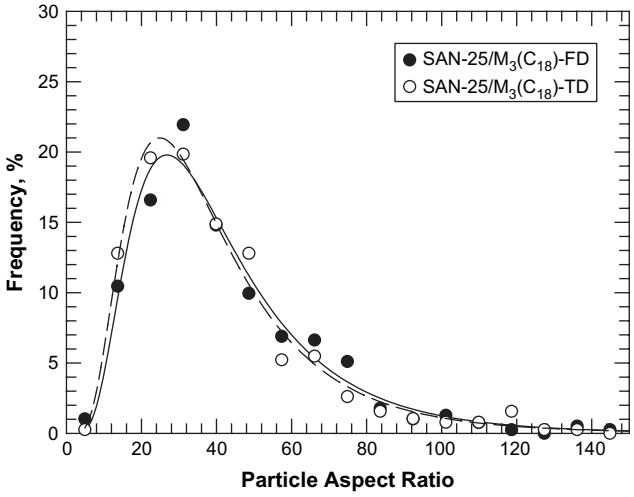

Fig. 11. Histograms showing distributions of individual particle aspect ratios for >350 particles, as measured from TEM images viewed along the transverse direction (TD) and flow direction (FD), for the SAN-25 nanocomposite. Histograms for the PS and SAN-13.5 nanocomposite aspect ratios were similar.

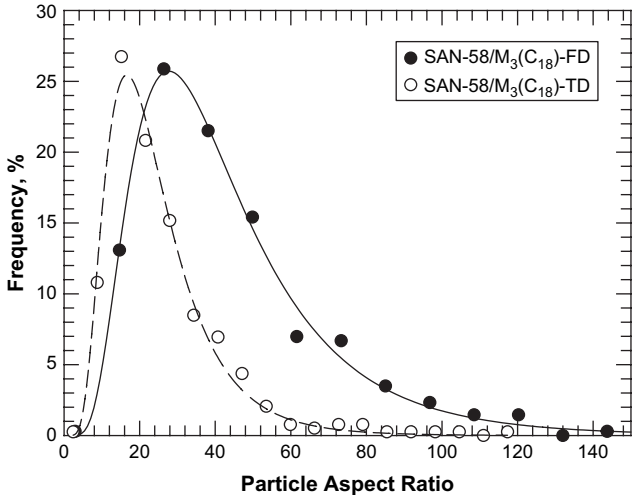

Fig. 12. Histograms showing distributions of individual particle aspect ratios for >350 particles, as measured from TEM images viewed along the transverse direction (TD) and flow direction (FD), for the SAN-58 nanocomposite. The lower measured average aspect ratio of the particles in the transverse direction is thought to arise from discrepancies inherent in measuring the thickness of irregularly-shaped particles.

directions may be due to longer particle lengths noted when viewed along the flow direction.

An areal particle density may be calculated from the TEM images simply by summing the number of particles observed in all of the TEM images for a given composite and dividing by the total area these images represent. Since incomplete particles appear at the edges of all images, and at low particle densities these may contribute significantly to the particle count (~10% in practice for the images seen here), we have simply counted all full particles in the image plus all incomplete particles on two of the four image edges. These values are reported in Table 2. While there are differences in particle densities depending on the direction of viewing that are difficult to rationalize, some useful trends emerge. Clearly the PS-based composites are much lower in particle density than the SAN-based composites. Further, the highest specific particle density reported, ~8 particles/μm^2, is still an order of magnitude lower than the values of 120–130 particles/μm^2 reported by Chavarria and Paul for well-exfoliated nylon 6/MMT nanocomposites blended with a pilot-scale twin-screw extruder [24].

Another morphological parameter which can be obtained from the TEM images using the Gatan DigitalMicrograph software is the angle of each particle with respect to the horizontal axis of the image, α; this axis does not, in general, coincide with any fixed direction within the molded bar since it is difficult to track the sense of direction during all the steps involved in obtaining the image. Thus, information about the actual flow direction is not preserved with the image. We can instead calculate an average angle of orientation for the particles. The relationship between the image-based angle of orientation, α, and the calculated average angle, $\bar{\alpha}$, is shown in Fig. 13.

The angle recorded by the system will have positive and negative values depending on the sense of tilt with respect to the horizontal axis of the image. This was resolved in the data collection by simply adding 180° to any negative reading.

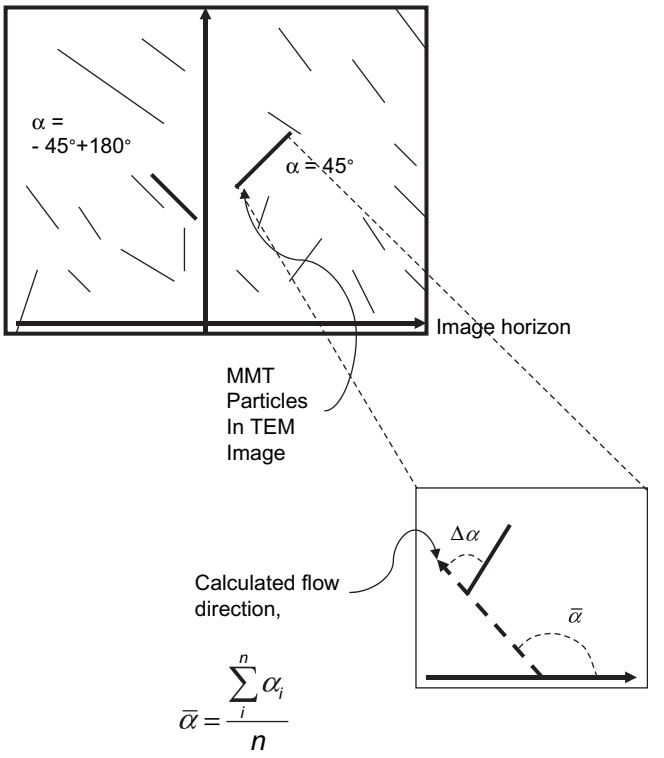

Fig. 13. Example of how the average particle deviation angle, Δα, was obtained from TEM image analysis.

An average angle, $\bar{\alpha}$, unique to each image, is obtained by algebraically summing the values and dividing by the total number of particles. The value so obtained should indicate the geometrical direction relative to the image axis. The absolute value of the deviation for each particle in the image relative to this direction is given by:

$$\Delta\alpha = |\alpha_i - \bar{\alpha}| \tag{4}$$

Deviation values for particles in all the images were averaged, $\langle\Delta\alpha\rangle$, and the average represents the randomness in orientation for the particles in the composite.

The $\langle\Delta\alpha\rangle$ values shown in Table 2 indicate much smaller deviations from the main angle of orientation for particles aligned in the flow direction (viewed in the transverse direction). This is consistent with the greater shear stresses expected along the flow direction.

In summary, the particle dimensions obtained from digital image analysis of these TEM photomicrographs indicate that there may be a slight maximum in the particle aspect ratio for composites with about 38% acrylonitrile in the copolymer, and that the PS and SAN-2-based composites, with low particle densities and high particle thicknesses, are the poorly exfoliated systems compared to the other SAN-based materials.

4.2. Wide angle X-ray scattering

The WAXS scans for the composites with various AN contents are shown in Fig. 14. The corresponding pristine organoclay ($M_3(C_{18})_1$) WAXS scan is shown at the bottom of Fig. 14;

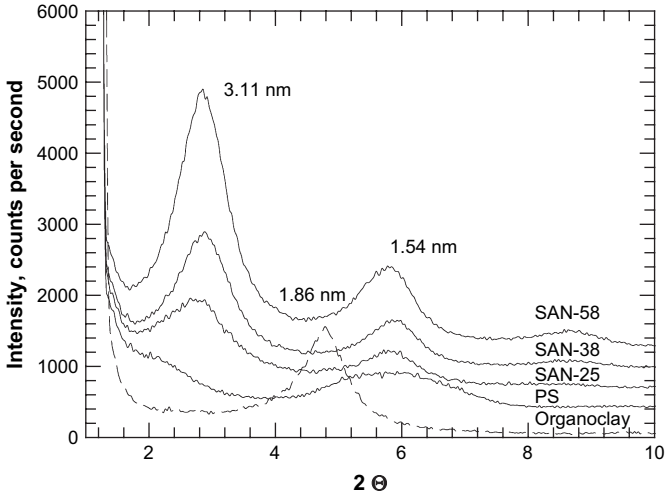

Fig. 14. WAXS scans for SAN/$M_3(C_{18})_1$ composites where weight percent of acrylonitrile in the copolymer is indicated. All composites contain 3.2% MMT. The lowest WAXS scan is for the pristine organoclay, and all other scans are shown with baselines incremented by 300 cps for clarity.

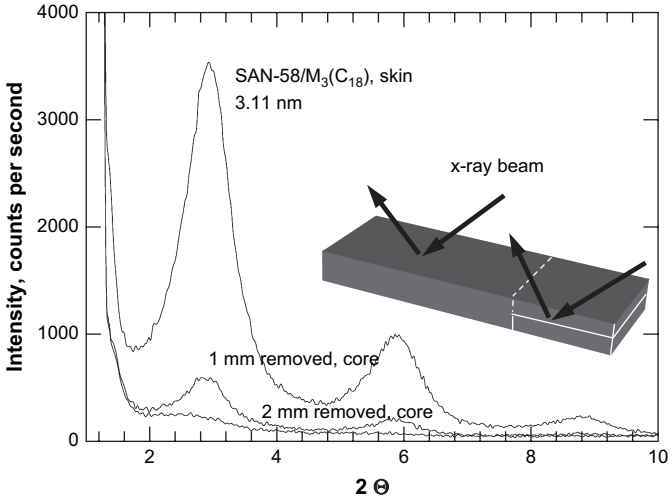

Fig. 15. WAXS scans for SAN-58/$M_3(C_{18})_1$ composite, the skin of the injection-molded bar has been milled off for the scans with lower peak intensity. Peak intensity is lowest in the core of the bar, indicating less particle orientation.

the other scans are shifted by successive increments to more clearly show the effect of the acrylonitrile in the copolymer. The PS-based composite exhibits a slightly higher average d_{001}-spacing than the other formulations, but peak broadening and asymmetry make it difficult to establish the exact peak location. The AN content did not affect the shift in the gallery spacing, Δd_{001}, for copolymers within the commercially important range near 25 wt%. Thus, there is little difference in intercalation behavior in this region.

The d_{001} peak height increases with acrylonitrile content. If the peak heights were primarily influenced by the number of exfoliated crystallites, one might conclude from WAXS data alone that the PS-based composites were more exfoliated than the SAN-58-based composites. This is not consistent, however, with the TEM results.

Note that the WAXS scans in Fig. 14 were obtained from the skins of injection-molded bars. The MMT particles being probed are more aligned in the skin than in the core where the TEM images were taken. Such orientation of the particles is expected to increase the WAXS peak height [2]. Fig. 15 compares the WAXS results from the SAN-58 standard bar (where the beam probes the skin of the bar) with WAXS results from bars which were precision milled to two different depths, corresponding to 3/4 and 1/2 of the original bar thickness. Clearly the clay particles in the core of the injection-molded bar do not produce the strong d_{001} peak that particles in the skin do, and this response varies with the thickness of the bar. Therefore, the WAXS data appear to be more influenced by the particle orientation in the skin of the bars rather than the extent of exfoliation.

5. Comparison of reinforcement effect for SAN-based nanocomposites

A direct comparison of the composite moduli as a function of weight percent of MMT for the various copolymers is presented in Fig. 16. Clearly the SAN-58-based nanocomposite shows a greater absolute modulus enhancement. However, interpretation of such results in terms of degree of exfoliation must be done with some care.

According to composite theory, the slope of the curves shown in Fig. 16 should be a function of the geometry of the particles, *i.e.*, aspect ratio, and the properties of the two components; montmorillonite platelets are assumed to have a modulus of 178 GPa [4] while the modulus of the styrenic copolymers ranges from 3.0 to 3.7 GPa. The reinforcement effect or slope of the relation between modulus and filler volume fraction is simply a line connecting these two moduli for the simplest case of an infinite aspect ratio such as a continuous fiber. This limiting case demonstrates that the modulus enhancement, or reinforcement, changes if the polymer modulus changes. Thus, the potential for reinforcement depends on the intrinsic properties of the polymer. Comparison of the

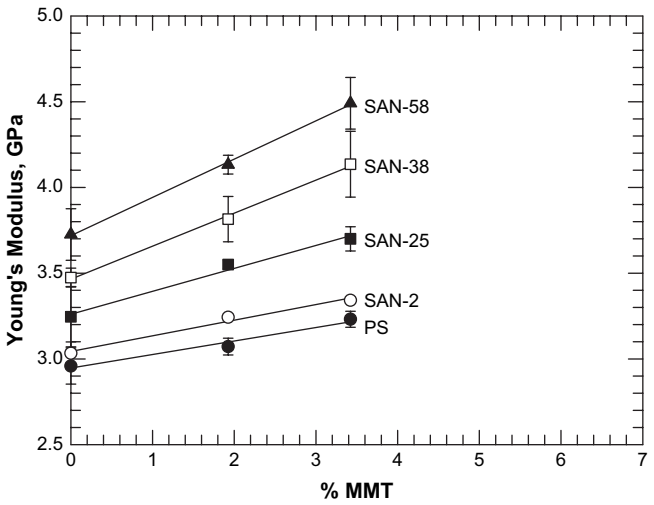

Fig. 16. Young's modulus for composites of SAN/MMT formed from various acrylonitrile contents (wt%) of the SAN copolymer.

reinforcement effects for composites based on different polymers must carefully account for this difference in potential for reinforcement. Use of a reinforcement factor, discussed previously, is appropriate when the matrix moduli vary over a limited range, which is the case for the SAN matrix copolymers in this study [7]. The reinforcement factors, RF_w, are simply the slope of the normalized modulus of the composite *versus* MMT content,

$$RF_w = \lim_{w_{platelets} \to 0} \frac{d[E/E_m]}{dw_{platelets}} \quad (5)$$

Eq. (5) is based on weight fraction of the filler ($w_{platelets}$), defined as such for practical reasons, but is easily converted to a reinforcement factor based on the volume fraction (RF), a parameter used in model predictions [7]. The reinforcement factors (RF_w) for the SAN-based nanocomposites, shown as filled circles in Fig. 17, indicate that the extent of reinforcement increases with acrylonitrile content in the copolymer even after the effect of the modulus matrix is accounted for, and there may be a slight maximum in that relationship.

Fig. 17 also shows for comparison a predicted reinforcement factor for materials which exhibit excellent dispersion, where aspect ratio is assumed for the purposes of this study to reach 100. This value is taken from studies by Fornes and Paul, indicating that for well-exfoliated montmorillonite organoclay dispersed in nylon 6 using a high-shear pilot-scale twin-screw extruder, the number average aspect ratio is very near 100 [4]. The prediction is made using Mori–Tanaka composite theory. One form of the Mori–Tanaka model which is suitable for the reinforcement caused by a disk-shaped filler oriented in the load direction has been discussed in greater detail elsewhere [4,25]. We assumed a Poisson's ratio of 0.36 for all polymers. Comparison of experimental values to Mori–Tanaka predictions for the well-exfoliated case indicates that these materials are not well exfoliated, which is in agreement with the overall TEM image analysis results and the previous discussion of areal particle densities.

6. Effect of matrix viscosity and shear stress on exfoliation

When considering the data presented above, it is important to realize that polarity of the polymer is not the only variable changing as the AN content of the matrix polymer is increased. As shown in Fig. 18, increasing AN content leads to significant increases in the melt viscosity of the polymer as indicated by the axial force measured at a given screw speed in the DSM microcompounder. Because of this increase in the melt viscosity, the MMT particles experience greater shear stress during mixing, which may be responsible for some of the observed enhancement in particle dispersion.

The shear stress during compounding can be increased independently of copolymer composition by increasing the rotational speed of the screws. (Note that in the DSM microcompounder, changing screw speed does not affect the residence time, unlike the case of a typical extruder.) If enhancement in composite reinforcement is primarily due to polymer-filler compatibility issues, then increasing the screw speed should not have a large effect on the resulting reinforcement factors. Conversely, if the particles are dispersed better at higher AN content simply because the melt viscosity/shear stress of the system is greater, then reinforcement factors will not only improve with increased screw speed, but also all RF_w should correlate with shear stress (measured as an axial force) independently of how the shear stress was generated.

Fig. 19 shows the RF_w for nanocomposites as a function of both acrylonitrile content and increasing screw speed. Clearly increasing screw speed causes the reinforcement levels to increase, and this effect appears to be significant. In Fig. 20, we see that the RF_w do not all collapse to a single relationship dependent solely on the plateau force. Therefore, increases in shear stress can improve the extent of exfoliation for these

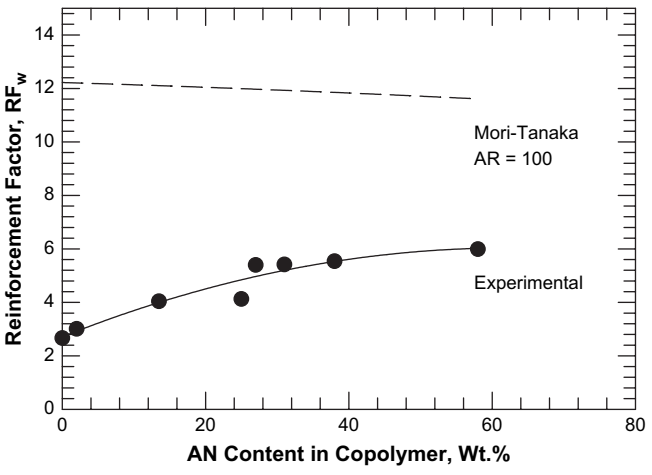

Fig. 17. Comparison of experimentally-determined reinforcement factors (RF_w) for composites of SAN/MMT formed from various acrylonitrile content in the copolymer to Mori–Tanaka predictions for a well-exfoliated nanocomposite where $E_{platelet} = 178$ GPa.

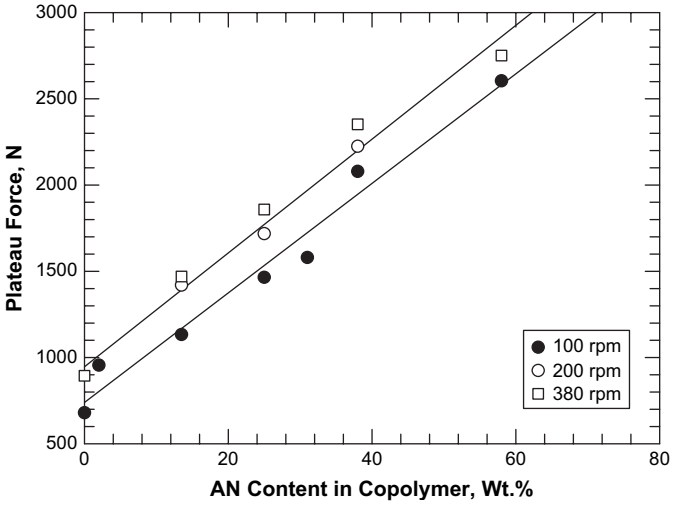

Fig. 18. Variation of the plateau force, a reflection of increasing melt viscosity, for the various acrylonitrile contents in the SAN copolymer at different screw speeds.

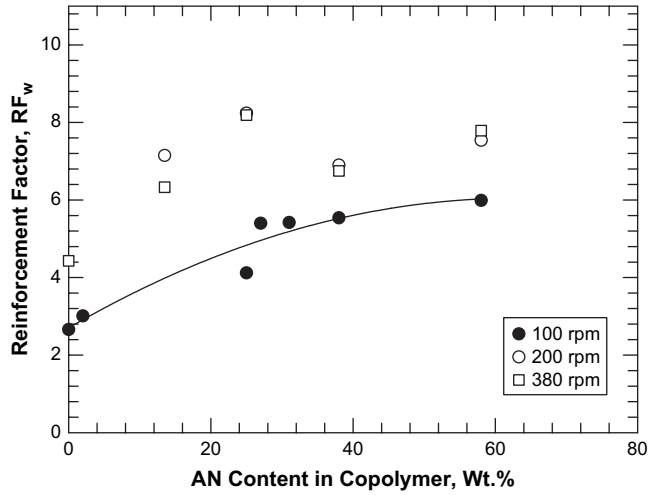

Fig. 19. Reinforcement factors, RF_w, for materials compounded at different screw speeds as a function of acrylonitrile content in the SAN copolymer. Note that increasing shear stress at constant acrylonitrile content has a significant effect on exfoliation.

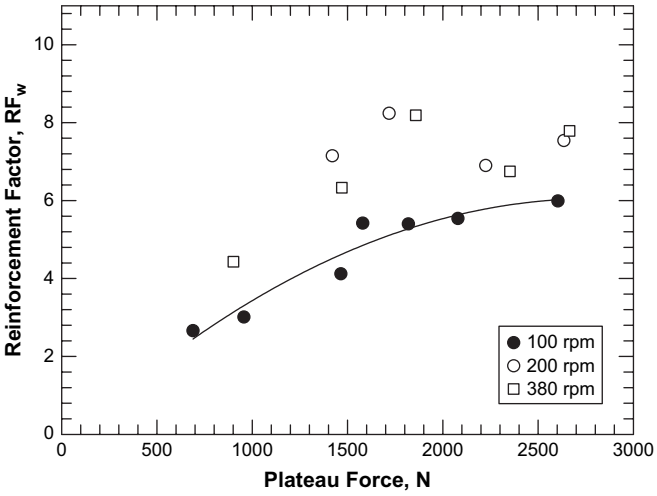

Fig. 20. Reinforcement factors, RF_w, for materials compounded at varying screw speeds and with varying acrylonitrile compositions, plotted as a function of the plateau axial force. Increasing shear stress with increasing screw speed clearly causes improved exfoliation, but acrylonitrile content is also a factor.

mixtures, but changes in the copolymer composition are also a factor determining filler dispersion and ultimately composite reinforcement.

7. Conclusions

The effect of the acrylonitrile (AN) content of poly(styrene-*co*-acrylonitrile) (SAN) on the morphology and properties of nanocomposites formed by melt mixing SAN with a single montmorillonite organoclay has been examined by several techniques. All the materials were processed on a DSM twin-screw microcompounder, and the resulting composite moduli are measured on injection-molded parts. Digital analysis of TEM photomicrographs indicate that there may be a slight maximum in particle aspect ratio for composites with about 38 wt% acrylonitrile (SAN-38), and that the PS-based composite demonstrates significantly higher particle thicknesses and lower specific particle densities, indicating a poorly exfoliated system compared to the other SAN-based composites. The specific particle densities for images from SAN-38 and SAN-58-based nanocomposites were $\sim$8 particles/μm^2, compared to values of $\sim$120 particles/μm^2 reported for well-exfoliated nylon 6-based nanocomposites by Chavarria and Paul [24]. Modulus enhancement, measured as the slope of the normalized modulus *versus* MMT content, was shown to increase with increasing acrylonitrile content. Increased AN content in the copolymer led to measurable increases in melt viscosity and, therefore, increased the shear stress on the particles during mixing. Reinforcement values for composites formed at various screw speeds did not fully correlate with either increased shear stress (as represented by the measured axial force developed by the screws during compounding) or the AN content in the copolymer, thus, both factors are important in determining filler dispersion and ultimately composite reinforcement.

Acknowledgements

The authors would like to thank the Air Force Office of Scientific Research for funding. We gratefully acknowledge interactions with the staff of Southern Clay Products, who provided materials and advice, including the WAXS performed by Tony Gonzales. Dr. JP Zhou at the Center for Nano and Molecular Science and the Texas Materials Institute, University of Texas at Austin provided electron microscopy support. Thanks to Bayer, Dow Chemical, Asahi and Monsanto for the SAN.

References

[1] Stretz HA, Paul DR, Keskkula H, Li R, Cassidy PE. Polymer 2005;46(8):2621.
[2] Vaia RA, Liu W. J Polym Sci Part B Polym Phys 2002;40:1590.
[3] Vermogen A, Masenelli-Varlot K, Seguela R. Macromolecules 2005;38:9661.
[4] Fornes TD, Paul DR. Polymer 2003;44:4993.
[5] Sheng N, Boyce MC, Parks DM, Rutledge GC, Abes JI, Cohen RE. Polymer 2004;45:487.
[6] Fornes TD, Paul DR. Macromolecules 2004;37:7698.
[7] Stretz HA, Paul DR. Polymer 2005;46:3818.
[8] Fornes TD, Yoon PJ, Keskkula H, Paul DR. Polymer 2001;42:9929.
[9] Chung IJ, Choi YS. Polymer 2004;45:3827.
[10] Choi YS, Wang KH, Xu M, Chung IJ. Chem Mater 2002;14:2036.
[11] Wilkie CA, Bourbigot S, Gilman JW. Polym Degrad Stab 2004;84:483.
[12] Giannelis EP, Weimer MW, Chen H, Sogah DY. J Am Chem Soc 1999;121:1615.
[13] Lee YS, Yoon BH, Nahm KS, Uthirakumar P. Eur Polym J 2004;40:2437.
[14] Morgan AB, Harris JD. Polymer 2004;45:8695.
[15] Tanoue S, Utracki LA, Garcia-Rejon A, Tatibouet J, Cole KC, Kamal MR. Polym Eng Sci 2004;44(6):1046.
[16] Tanoue S, Utracki LA, Garcia-Rejon A, Sammut P, Ton-That M-T, Pesneau I, et al. Polym Eng Sci 2004;44(6):1061.
[17] Galvin ME, Beyer FL, Beck Tan NC, Dasgupta A. Chem Mater 2002;14:2983.
[18] Vaia RA, Gianellis EP. Macromolecules 1997;30:8000.

[19] Robello DR, Yamaguchi N, Blanton T, Barnes C. J Am Chem Soc 2004; 126:8118.
[20] Morgan AB, Beach MW, Harris JD, Anderson SK, Chu L-L. Polymer 2004;45:4051.
[21] Ko MB. Polym Bull 2000;45:183.
[22] Goettler LA, Nagaraj PT. Polymer processing society. Melbourne, Australia; 2003.
[23] Suter UW, Osman MA, Ploetze M. J Mater Chem 2003;13:2359.
[24] Chavarria F, Paul DR. Polymer 2004;45:8501.
[25] Tandon GP, Weng GJ. Polym Compos 1984;5(4):327.